Manipulability Analysis

Nikolaus Vahrenkamp*†, Tamim Asfour*, Giorgio Metta†, Giulio Sandini† and Rüdiger Dillmann*
* Institute for Anthropomatics, Karlsruhe Institute of Technology (KIT), Karlsruhe, Germany
† Robotics, Brain and Cognitive Sciences Departement, Istituto Italiano di Tecnologia (IIT), Genova, Italy

***Abstract*—The ability of computing a quality index for given configurations can be useful for several applications in the context of robotic manipulation. E.g. it can be used for monitoring the current state of the system or it can support decision processes, such as grasp selection in humanoid robotics. Here, a large set of precomputed grasps for a given object have to be quickly filtered in order to select the reachable sub set, for which the inverse kinematics (IK) problem has to be solved. In this work, we present an approach for analyzing the workspace capabilities of a manipulator in order to store a representation for efficient online processing. Compared to existing work, where usually reachability information is used to represent the robot's capabilities, we show how an extended manipulability measure can be used to build a quality distribution in workspace. The proposed approach for manipulability measurement is suitable for redundant manipulators while considering joint limits and self-distance. Further, task specific distributions are introduced and several applications for the humanoid robots ARMAR-III [1] and iCub [2] are presented.**

I. Introduction

The ability of supervising own movements is essential for robots operating in such different domains as industrial applications, service or humanoid robotics. Hence, the systems must be equipped with methods to measure their performance, accuracy or success rate. In this context, measuring the manipulability is a well-known technique for determining the ability to maneuver in workspace.

The manipulability index of given robot poses, introduced by Yoshikawa in 1985 [3], can be calculated as a quality value that gives information about how good an adjustment in workspace is possible. With such information, redundancy of the robot can be exploited to favor poses which result in higher manipulability and which hence allow better adaption during execution. In case the manipulability is used to support a decision process, e.g. when a grasp should be selected out of a set of potential grasps, a precomputed representation can be useful in order to serve manipulability queries efficiently.

Several approaches of determining the reachability of manipulators are known in literature, which are based on the idea that a voxelized 3D or 6D grid is filled with reachability information (see [4], [5], [6]). Due to the discretized representation the reachability entries can just give a hint, whether a pose in workspace will lead to a valid IK solution or not. In this work we will show, how a similar data structure can be used to capture the manipulability distribution of a manipulator in workspace. The resulting data therefore extends the approximated reachability information with a quality index. This additional information can be used to support grasp selection in manipulation tasks (see Fig. 1) in order to favor grasps that result in a high manipulability. High manipulability allows to adapt movements during execution, e.g. when visual servoing approaches are used to improve the accuracy [7]. The proposed algorithms are published within the open-source robotics toolbox Simox, which can be accessed online[1].

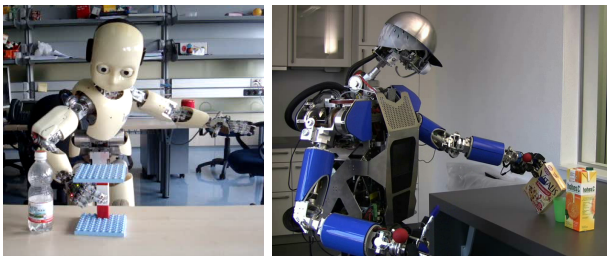

Fig. 1. The humanoid robots iCub and Armar-III performing grasping tasks in cluttered environments.

A. Manipulability Measure

With Yoshikawa's manipulability index [3] a quality measure for redundant manipulators was introduced, which describes the distance to singular configurations. The approach is based on analyzing the manipulability ellipsoid that is spanned by the singular vectors of the Jacobian. In [3] the manipulability measure is proposed as

$$w = \sqrt{det(JJ^T)} = s_1 s_2 \cdots s_n. \quad (1)$$

Since w can be rewritten by multiplying the singular values s_i, the measure is proportional to the volume of the manipulability ellipsoid. The *inverse condition number* measurement was introduced in [8] as the relation of the smallest to the largest singular value

$$c = \frac{1}{cond(J)} = \frac{s_n}{s_1}. \quad (2)$$

In [9], the following penalization was introduced to consider the distance to the lower (l_j^-) and the upper (l_j^+) joint limits:

$$P(\theta_j) = 1 - \exp(-k \prod_{j=1}^{n} \frac{(\theta_j - l_j^-)(l_j^+ - \theta_j)}{(l_j^+ - l_j^-)^2}). \quad (3)$$

In this penalty function k is a scaling factor that can be used to adjust the behavior near joint limits. By multiplying the manipulability with P, configurations which are near joint

[1] http://simox.sourceforge.net

limits are penalized, but redundancy is not considered, which can lead to an erroneous quality information (e.g. one joint is close to a boundary while the end effector's maneuverability is not affected due to redundancy).

A task specific quality function for a redundant manipulator is considered in [10] in order to compute optimal poses.

A dexterous performance measure is presented in [11]. By analyzing the so-called augmented Jacobian matrix, which combines information about the position, orientation, and joint limits of the end-effector, the manipulability of joint configurations can be measured. It is shown that this approach is more accurate than Yoshikawa's manipulability measure and exemplary applications for optimizing base placements are given. However, the approach relies on the generation of surface patches to represent the reachable workspace, which can lead to challenging computational problems. Joint velocity limits can be considered [12], resulting in an analysis of a scaled Jacobian.

As shown in [12] or [13], the use of manipulability ellipsoids can lead to issues that are caused by mixing translational and rotational sub spaces for manipulability measurement. By using manipulability polytopes the described problems can be avoided, but higher computational costs have to be taken into account. In this work, we use a weighting matrix W_x in order to set the translational components of the Jacobian matrix in relation with the rotational components (see [13]).

B. Precomputed Reachability Information

In literature the reachability of a manipulator is loosely defined as the volume of the workspace that can be reached by the end effector. Usually the three- or six-dimensional Cartesian space around the robot is investigated, whereas only the position (3D) or position and orientation (6D) is considered. The reachability data is created by filling a voxelized data structure in an offline step. The grid entries represent either a probability that a given pose that lies within the corresponding workspace voxel is reachable or binary information is used to indicate that a voxel lies (partly) within the reachable workspace (see [4], [5], [6]).

In this work we pick up the idea of having a precomputed workspace representation of a manipulator. Instead of holding information about the reachability, we store a quality index that serves information about the manipulability in workspace (see Sec. III).

II. Extended Manipulability Measure

In this work we use an extended manipulability measurement in order to consider constraints that limit the maneuverability in workspace. Such constraints are introduced by joint boundaries and workspace (self-)collisions, but any other constraints can be incorporated as long as the derivation with respect to joint movements can be built.

In the context of optimal control, several approaches are known to avoid joint limits and obstacles [14], [15]. Compared to these works, we are not interested to find an optimal control strategy for a requested end effector movement, but we want to investigate the limitations that are given for any possible movements in workspace.

A. Joint Limit Penalization Function

The influence of joint limits on the manipulability measure can be considered by analyzing a modified Jacobian matrix J. The entries of J are penalized according to the quality measure that arises from the current distance to joint limits (l_j^- and l_j^+). Since the distance to lower or upper joint limit usually differs, the corresponding penalization terms also differ and hence, the quality measure depends on the investigated workspace movement.

In [14] a joint limit potential function $h(\theta)$ is proposed and the joint limit gradient function $\bigtriangledown h(\theta)$ is derived. For each joint θ_j the corresponding entry of $\bigtriangledown h(\theta)$ can be with

$$\bigtriangledown h(\theta)_j = \frac{\partial h(\theta)}{\partial \theta_j} = \frac{(\theta_j - l_j^-)^2(2\theta_j - l_j^+ - l_j^-)}{4(l_j^+ - \theta_j)^2(\theta_j - l_j^-)^2}. \quad (4)$$

This gradient is equal to zero, if the joint is at the middle of its range and goes to infinity at either limit. It can be used to avoid joint limits during online control as shown in [14] or [15]. In order to construct an according penalization term we have to distinguish the different potential movement directions in workspace (see Sec. II-C). Depending of the actual position of the joint (either located in the lower or the upper half of its range), the following two penalization terms are built:

$$p_j^- = \begin{cases} 1, & |\theta_j - l_j^-| > |l_j^+ - \theta_j| \\ \frac{1}{\sqrt{1+|\bigtriangledown h(\theta)_j|}}, & otherwise \end{cases}$$
$$p_j^+ = \begin{cases} \frac{1}{\sqrt{1+|\bigtriangledown h(\theta)_j|}}, & |\theta_j - l_j^-| > |l_j^+ - \theta_j| \\ 1, & otherwise \end{cases} \quad (5)$$

In Eq. 5, the penalization term p_j^- stands for the penalization that has to be applied when investigating the joint's movement in negative direction. If the current joint value is located in the upper half of its range, the value is 1, which means that the movement does not underlie any penalizations. Otherwise, the movement is penalized according to Eq. 4. The second part of Eq. 5, describes the construction of p_j^+, the penalization term that is applied when a movement in positive joint direction is investigated. In this case, the penalization is only considered when the current joint position is located in the upper half of its range.

B. Obstacle Penalization Function

Obstacles, such as environmental objects or parts of the robot, limit the possibility of a manipulator to maneuver in workspace. Hence, the manipulability measure should consider a penalization that is derived from the distance and the position of any limiting obstacles. By determining the nearest points p_o and p_m on the surface of the obstacle and the manipulator, one can determine the corresponding obstacle vector $v' = p_o - p_m$ and the obstacle distance

$d = |v'|$. The vector $v \in \mathbb{R}^3$ is extended to $\mathbb{R}^6$ by setting the rotational components to zero: $v = [v_0, v_1, v_2, 0, 0, 0]^T$.

A collision function $P(\theta, d)$ should go to infinity for $d \to 0$ and decays exponentially to zero as d increases. As proposed in [15], we choose

$$P(\theta, d) = e^{-\alpha d} d^{-\beta}. \tag{6}$$

The parameters α and β can be used to adjust the obstacle influence (see [15] for details). The gradient of P is the collision gradient function, which gives information about how each joint influences the obstacle distance:

$$\bigtriangledown P(\theta, d) = \frac{\partial P}{\partial \theta} = \left[\frac{\partial P}{\partial \theta_1}, \ldots, \frac{\partial P}{\partial \theta_n}\right] = \frac{\partial P}{\partial d}\frac{\partial d}{\partial \theta}. \tag{7}$$

As shown in [15] $\bigtriangledown P$ can be computed with

$$\begin{array}{l} \frac{\partial P}{\partial d} = -e^{-\alpha d} d^{-\beta}(\beta d^{-1} + \alpha), \\ \frac{\partial d}{\partial \theta} = \frac{1}{d}\left[J^T v\right]^T. \end{array} \tag{8}$$

Finally, two penalization terms can be constructed similar to Eq. 5. Again, we are interested in all potential movements of the end effector and therefore a distinction is made, whether a workspace movement in negative ($o^-_{i,j}$) or positive ($o^+_{i,j}$) direction is investigated:

$$\begin{array}{l} o^-_{i,j} = \left\{ \begin{array}{rl} 1, & v_i > 0, i > 3 \\ \frac{1}{\sqrt{1+|\bigtriangledown P_j|}}, & otherwise \end{array} \right. \\ o^+_{i,j} = \left\{ \begin{array}{rl} \frac{1}{\sqrt{1+|\bigtriangledown P_j|}}, & v_i > 0, i \leq 3 \\ 1, & otherwise \end{array} \right. \end{array} \tag{9}$$

In Eq. 9 the terms $o^-_{i,j}$ and $o^+_{i,j}$ represent the penalizations that have to be applied when investigating movements in negative respectively positive Cartesian directions. Penalizations are only applied for translational dimensions ($i \leq 3$) and if the obstacle is located in the corresponding direction (v_i).

C. Computing the Augmented Jacobians

Compared to [14] or [15], we cannot use the gradients directly since an explicit movement $x \in \mathbb{R}^6$ is needed in order to optimize the control law. In the context of manipulability, we are interested in a measurement that serves information about the possibility to maneuver in workspace and hence all potential movements must be covered. Since the manipulability is affected by joint limit and obstacle constraints and, as shown above, these constraints directly depend on the investigated movement, we have to build a representation that covers all potential directions. Therefore, the space of workspace movements is partitioned by 2^6 hyperoctants, which are identified by $\Gamma \in \{-1, +1\}^6$. For each Γ an augmented Jabobian matrix $\tilde{J}$ is built by considering the corresponding penalization terms. Finally, the manipulability of $\tilde{J}$ is computed, which gives information about the manipulability of all potential movement directions that are represented by the corresponding hyperoctant Γ.

1. Joint Limit Penalization Matrix

Depending on the investigated movement of θ_j, either p^-_j (move towards lower joint limit) or p^+_j (move towards upper joint limit) can be applied in order to penalize the computed maneuverability. Therefore, the following penalization matrix is computed:

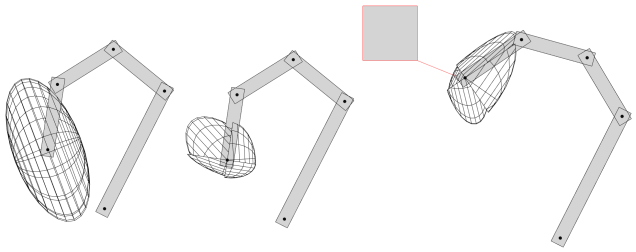

Fig. 2. (a) The classical manipulability ellipsoid without joint limit penalization ($c = 0.170$). (b) For each quadrant different penalization terms are applied according to the corresponding joint limit influence ($\tilde{c}_{ext} = 0.047$). (c) The obstacle influences the penalization terms ($\tilde{c}_{ext} = 0.067$).

$$L_{i,j}(\Gamma, \theta) = \left\{ \begin{array}{ll} p^-_j, & \mathrm{sgn}(J_{i,j}(\theta))\,\mathrm{sgn}(\Gamma_i) < 0 \\ p^+_j, & otherwise \end{array} \right. \tag{10}$$

The selection which penalization has to be applied depends on two facts. Firstly, the sign of the corresponding Jacobian entry $J_{i,j}$ indicates the direction a positive Cartesian movement causes in joint space. Further, the sign of i-th entry of Γ indicates which hyperoctant is considered. E.g. a positive sign of $J_{i,j}$ and a hyperoctant in a negative coordinate axis results in a joint space movement towards the negative joint limit and hence, p^-_j has to be considered for penalization.

2. Collision Penalization Matrix

In addition, collision penalizations can be computed. Here, either o^-_i (movement in negative coordinate axis) or o^+_i (movement in positive coordinate axis) are considered:

$$O_{i,j}(\Gamma, \theta) = \left\{ \begin{array}{ll} o^-_{i,j}, & \mathrm{sgn}(\Gamma_i) < 0 \\ o^+_{i,j}, & otherwise \end{array} \right. \tag{11}$$

3. The Augmented Jacobian

Finally, the augmented Jacobian $\tilde{J}$ is constructed as follows:

$$\tilde{J}_{i,j}(\Gamma, \theta) = L_{i,j}(\Gamma, \theta) O_{i,j}(\Gamma, \theta) J_{i,j}(\theta). \tag{12}$$

By applying Eq. 12 to all possible permutations of Γ, 64 Jacobians are generated, each of which describes the maneuverability in the corresponding hyperoctant of the workspace. These matrices can be analyzed for manipulability in order to retrieve a quality index for a given configuration. Therefore all Jacobians are decomposed via Singular Value Decomposition (SVD) in order to retrieve the corresponding sets of singular values $\tilde{s_\Gamma}$. To compute the *Extended Inverted Condition Number* the minimum and maximum singular value is determined:

$$\tilde{c}_{ext} = \frac{min\{\tilde{s_\Gamma}\}}{max\{\tilde{s_\Gamma}\}}. \tag{13}$$

The quality measure $\tilde{c}_{ext}$ implicitly considers redundancy, since a penalization due to joint limits can be compensated by redundant joints in the kinematic structure. The results of this measure applied to a 4 degrees of freedom (DoF) planar manipulator can be seen in Fig. 2. The figure on the

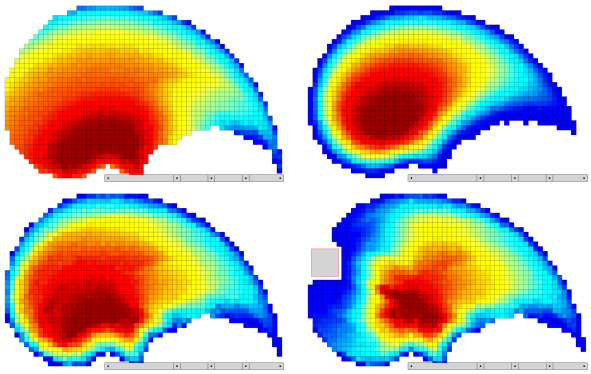

Fig. 3. Top row: (a) The distribution of the classical manipulability measure is analyzed for a planar 4 DoF robot. (b) By applying a global penalization term, joint limits can be considered, but redundancy is not reflected by the measure. Bottom row:(c) The distribution of the extended manipulability measure $\tilde{c}_{ext}$ in workspace. (d) The obstacle is considered additionally.

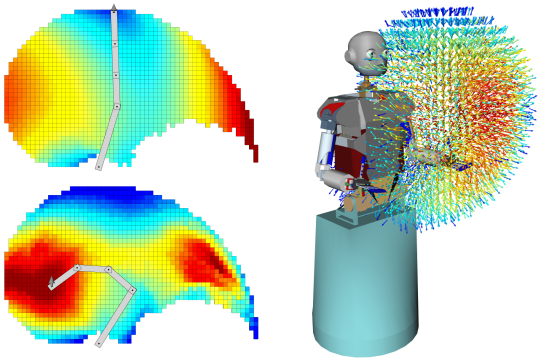

Fig. 4. (a) The task specific manipulability distribution for an upright prototype direction without considering joint limits (top). The distribution of the task specific manipulability $\tilde{c}_p$ (bottom). (b) The task-specific manipulability distribution for the left arm of ARMAR-III considering an upright lifting movement.

left shows a 2D visualization of the manipulability ellipsoid without considering joint limits, whereas the second visualization shows the scaled manipulability ellipsoids in each of the four quadrants. On the right, an obstacle is considered and the minimum distance is visualized. The according joint limit and obstacle penalization terms are applied as described in Eq. 12. Note, that only parts of the manipulability ellipsoids are visualized, so that one can see the penalization effects in the different quadrants. Due to this visualization technique, discontinuous transitions arise between the quadrants. Such artifacts only affect the visualization and have no influence on the computation, since for each quadrant (respectively hyperoctant in the general case) the whole manipulability ellipsoid is considered.

III. Manipulability Analysis

In order to build up a representation of the manipulability distribution in workspace, we propose a 6D voxelized data structure holding manipulability reference values in each voxel. Since the mapping between C-space and workspace is not unique for redundant manipulators, either the average manipulability or the lower respectively the upper bound of the achievable manipulability within a voxel can be stored. Hence, the manipulability data cannot be seen as an exact representation of the manipulators capabilities, but it can be used to efficiently serve an approximation of the expected manipulability of a given pose in workspace. This can be useful in several situations, e.g. when the selection of a grasp should be made and a large number of potential grasping poses are available. Further, the expected manipulability can help in choosing a suitable location for a hand-over process.

A workspace representation of the robot's reachability or manipulability capabilities can be built by two ways. Either work or joint space is discretized and all configurations are processed in order to update the corresponding 6D voxel, or randomized approaches are used. In the following, we build the manipulability representation by sampling a large set of configurations randomly. For each sample, the corresponding $\tilde{c}_{ext}$ value is computed and the 6D voxel v is determined by computing the forward kinematics of the manipulator in order to determine the location of the end effector. If the actual entry of v is lower than $\tilde{c}_{ext}$, the value is updated. This leads to an upper-bound representation of the achievable manipulability which can be seen as an optimistic view on the robot's possibility to maneuver in workspace.

Fig. 3 shows a visualization of the manipulability distribution of a 2D planar robot with 4 DoF. For each position that is indicated, the maximum manipulability is shown, whereas the color indicates the magnitude of the achievable manipulability (blue:low, red:high). On the top left the classical manipulability index c is used, whereas the top right figure shows the distribution when a penalization term according to Eq. 3 is applied when measuring the manipulability. Since redundancy is not considered in Eq. 3, the resulting distribution gives only limited information about the achievable manipulability of a redundant manipulator.

When applying the proposed penalizations, the corresponding distribution can be seen in Fig. 3. The bottom left figure shows the result when joint limits are penalized according to Eq. 10. On the bottom right figure, the obstacle penalization (Eq. 11) is additionally applied and the combined Jacobians are analyzed as described in Section II-C.

A. Task-Specific Manipulability Distributions

In case the robot is supposed to frequently execute a specific task, as it is the case e.g. for pick-and place operations, task-specific manipulability distributions can be precomputed in order to support the execution. Such distributions give information about the possibility to move in a specific direction $v_p \in \mathbb{R}^6$.

The penalization terms are computed according to Eq. 12, and since a hyperoctant ϵ_p is defined by the direction v_p, only one augmented Jacobian $\tilde{J}(\epsilon_p, \theta)$ has to be assembled. Further, the magnitude of the Jacobian's gradient with respect to the given prototype direction v_p is used as a quality index:

$$q_p(\theta) = |\tilde{J}(\epsilon_p, \theta)^T v_p|. \tag{14}$$

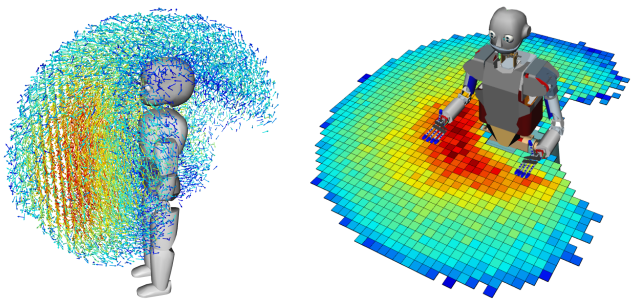

Fig. 5. (a) A 3D visualization of the 6D manipulability distribution of iCub's 10 DoF kinematic chain covering torso and right arm. (b) A cut through the manipulability distribution of the ARMAR-III's right manipulator (torso and arm). Joint limits and self-distance are considered by the underlying manipulability measure.

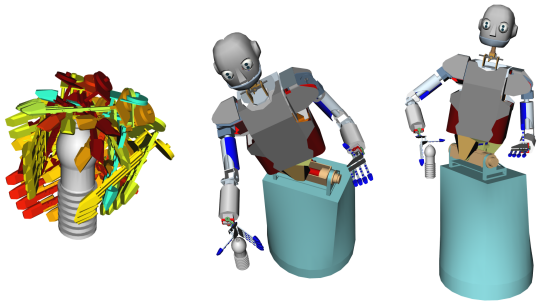

Fig. 6. (a) The manipulability of a set of reachable grasps is encoded by color. (b) A grasp with $\tilde{c}_{ext} = 0.02$. (c) The optimal grasp in terms of manipulability ($\tilde{c}_{ext} = 0.12$).

Together with the inverted condition number $\tilde{c}_{\epsilon_p}$ for the corresponding hyperoctant, the resulting manipulability can be computed with:

$$\tilde{c_p} = q_p(\theta)\tilde{c}_{\epsilon_p}. \tag{15}$$

The distribution of the corresponding manipulability values when considering an upright prototype direction v_p can be seen in Fig. 4(a). The distribution of the manipulability w.r.t. an upright movement for the left arm of ARMAR-III is shown in Fig. 4(b).

IV. Applications

A. Manipulability Distribution of Humanoid Robots

In Fig. 5 a 3D visualization of the manipulability distributions of iCub and ARMAR-III can be seen. In both cases the kinematic chain covering three torso and seven arm joints has been considered. The underlying manipulability measure incorporates penalizations due to joint limits and self distance as described in Sec. II. The left figure shows a 3D visualization of the 6D distribution, which was generated by showing the orientation with maximum manipulability at each 3D position. On the right, a cut through the 6D distribution is shown.

B. Performance Evaluation

The main advantage of an offline generated manipulability distribution is given by the possibility to structure the data in order to speed up information retrieval during online processing. In the following experiment we evaluate the effect of using precomputed manipulability representations in the context of grasp selection.

In Fig. 6 the model of a water bottle for which 1000 precomputed grasps are available can be seen on the left. An exemplary subset of reachable grasps is depicted, whereas the manipulability is encoded by color (blue:low, red:high). To measure the performance, the bottle is placed randomly in front of ARMAR-III and different strategies for grasp selection are evaluated. Firstly, no precomputed data is used and the IK-problem is solved for all grasps for the 10 DoF kinematic chain covering torso and arm. In case an IK-solution could be retrieved, the manipulability is computed for the corresponding joint configuration in order to determine the grasp with maximum $\tilde{c}_{ext}$. In the second approach all grasps are filtered according to their reachability. Here, reachability is given when the corresponding entry of the manipulability distribution is greater zero. This leads to a binary representation of the 6D reachability similar to the approaches of [4], [5], [6]. For the remaining sub-set of reachable grasps, the IK-solutions are computed in order to determine the corresponding manipulability. The third approach takes full advantage of the precomputed manipulability data. Due to the efficient data structures an ordered set of reachable grasps with corresponding manipulability values can be retrieved in less than one millisecond and the IK-problem has only to be solved for the first entry of this list (see Table I).

TABLE I
Comparison of different approaches for grasp selection (Average of 100 tests).

	Overall	Reach. / Manip. access	IK Solving	Manip. Comp.
No precomputed data	9.97s	-	9.07s	0.90s
Reachability data	2.24s	<0.001s	1.75s	0.49s
Manipulability data	0.01s	<0.001s	0.01s	-

C. Grasp Selection based on Manipulability

In this setup, manipulability distributions are used to support the grasp selection process, which is part of a grasping pipeline implemented on the humanoid robot iCub. The grasping pipeline takes advantage of offline generated data, such as object specific sets of grasps and manipulability data as proposed in this work. During online processing a subset of reachable grasps is determined according to the object's pose. Therefore, all grasps are transformed to Cartesian grasping poses by combining the object's pose in workspace with the object-grasp relation. These poses can then be quickly filtered according to their manipulability and the resulting ordered subset gives information about reachability and manipulability of the remaining grasps. In addition, the inverse kinematics (IK) problem is solved and a collision-free motion is generated with algorithms related

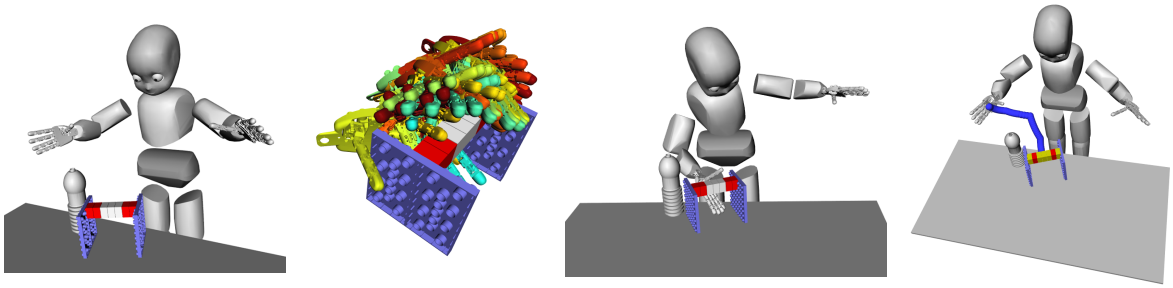

Fig. 7. iCub's grasping pipeline is supported by precomputed manipulability distributions. (a) The virtual representation of the scene. (b) All reachable grasps are colorized according to their manipulability. (c) The IK-solution of the selected grasp. (d) A collision-free grasping motion.

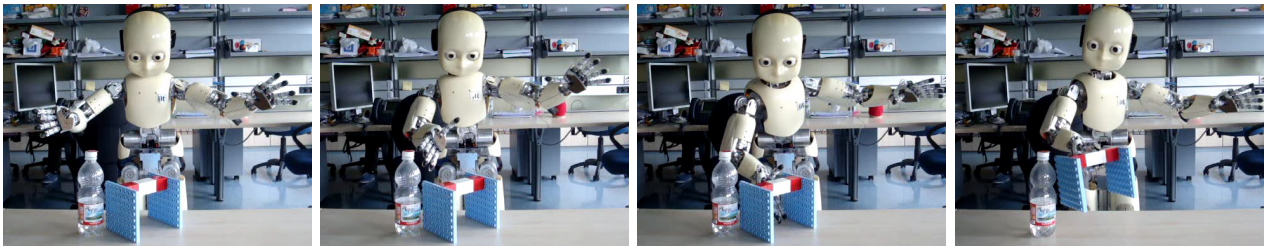

Fig. 8. The grasp selection of iCub's grasping pipeline is supported by precomputed manipulability distributions.

to Rapidly-exploring Random Trees (RRT) [16]. Fig. 7 depicts the results of the different processing stages and the execution on iCub is shown in Fig. 8.

V. Conclusion

In this work, we presented an integrated approach for determining the manipulability for redundant manipulators. We showed how classical measurements, which are mostly based on analyzing the manipulability ellipsoid, can be extended in order to consider constraints coming from joint limits, workspace obstacles or self-distance while explicitly considering redundancy. This extended manipulability measurement is used to build the distribution of a manipulator's manipulability in workspace, allowing to capture the capabilities of a robot in terms of operational freedom. In addition we showed how task specific data can be generated and how the manipulability data can be used for grasp selection on humanoid robots.

Acknowledgment

The research leading to these results has received funding from the European Union Seventh Framework Programme under grant agreement 270273 (Xperience).

References

[1] T. Asfour, K. Regenstein, P. Azad, J. Schröder, A. Bierbaum, N. Vahrenkamp, and R. Dillmann, "ARMAR-III: An integrated humanoid platform for sensory-motor control." in *IEEE-RAS International Conference on Humanoid Robots*, 2006, pp. 169–175.

[2] G. Metta, G. Sandini, D. Vernon, L. Natale, and F. Nori, "The icub humanoid robot: an open platform for research in embodied cognition," in *Proceedings of the 8th Workshop on Performance Metrics for Intelligent Systems*. New York, NY, USA: ACM, 2008, pp. 50–56.

[3] T. Yoshikawa, "Manipulability of robotic mechanisms," *The International Journal of Robotics Research*, vol. 4, no. 2, pp. 3–9, 1985.

[4] F. Zacharias, C. Borst, and G. Hirzinger, "Capturing robot workspace structure: representing robot capabilities," in *Intelligent Robots and Systems, 2007. IROS 2007. IEEE/RSJ International Conference on*, 29 2007-Nov. 2 2007, pp. 3229–3236.

[5] R. Diankov, "Automated construction of robotic manipulation programs," Ph.D. dissertation, Robotics Institute, Carnegie Mellon University, Pittsburgh, PA, September 2010.

[6] N. Vahrenkamp, D. Berenson, T. Asfour, J. Kuffner, and R. Dillmann, "Humanoid motion planning for dual-arm manipulation and re-grasping tasks," in *Intelligent Robots and Systems, IROS*, 2009.

[7] N. Vahrenkamp, S. Wieland, P. Azad, D. Gonzalez, T. Asfour, and R. Dillmann, "Visual servoing for humanoid grasping and manipulation tasks," in *Humanoid Robots, 2008. Humanoids 2008. 8th IEEE-RAS International Conference on*, Dec. 2008, pp. 406–412.

[8] M. Togai, "An application of the singular value decomposition to manipulability and sensitivity of industrial robots," *SIAM Journal on Algebraic and Discrete Methods*, vol. 7, no. 2, pp. 315–320, 1986.

[9] M.-J. Tsai, "Workspace geometric characterization and manipulability of industrial robots," Ph.D. dissertation, Ohio State University, 1986.

[10] B.-H. Jun, P.-M. Lee, and J. Lee, "Manipulability analysis of underwater robotic arms on rov and application to task-oriented joint configuration," in *OCEANS '04. MTTS/IEEE TECHNO-OCEAN '04*, vol. 3, nov. 2004, pp. 1548 –1553 Vol.3.

[11] K. Abdel-Malek, W. Yu, and J. Yang, "Placement of robot manipulators to maximize dexterity," *International Journal of Robotics and Automation*, vol. 19, no. 1, pp. 6–14, 2004.

[12] J. Lee, "A study on the manipulability measures for robot manipulators," in *Intelligent Robots and Systems, 1997. IROS '97., Proceedings of the 1997 IEEE/RSJ International Conference on*, vol. 3, sep 1997, pp. 1458 –1465 vol.3.

[13] R. Finotello, T. Grasso, G. Rossi, and A. Terribile, "Computation of kinetostatic performances of robot manipulators with polytopes," in *Robotics and Automation, 1998. Proceedings. 1998 IEEE International Conference on*, vol. 4, may 1998, pp. 3241 –3246 vol.4.

[14] T. F. Chan and R. Dubey, "A weighted least-norm solution based scheme for avoiding joint limits for redundant joint manipulators," *Robotics and Automation, IEEE Transactions on*, vol. 11, no. 2, pp. 286 –292, 1995.

[15] B. Dariush, G. Bin Hammam, and D. Orin, "Constrained resolved acceleration control for humanoids," in *Intelligent Robots and Systems, 2010 IEEE/RSJ International Conference on*, oct. 2010, pp. 710 –717.

[16] J. Kuffner and S. LaValle, "RRT-connect: An efficient approach to single-query path planning," in *IEEE Int'l Conf. on Robotics and Automation (ICRA'2000), San Francisco, CA*, 2000, pp. 995–1001.